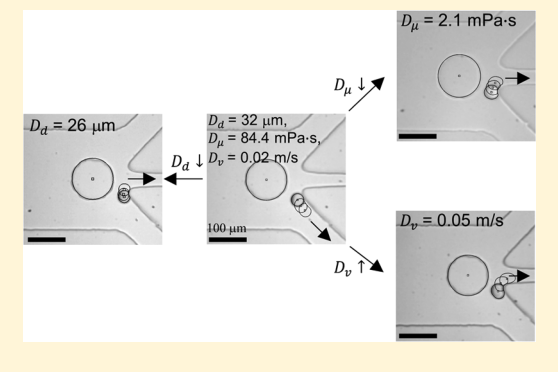


# **Deformation-Based Droplet Separation in Microfluidics**

Yunju Chang, <sup>†</sup> Xinye Chen, <sup>‡</sup> Yuting Zhou, <sup>§</sup> and Jiandi Wan\*, <sup>§</sup>

Supporting Information

**ABSTRACT:** Deformation-based particle/droplet separation is important in many industrial and medical applications. The roles of different physical parameters of particles/droplets such as viscosity, velocity, and size in the sorting process, however, remain elusive. Here, we designed a microfluidic device with a cylindrical post that can separate droplets depending on droplet size, viscosity, and velocity. We showed that droplets with a large size or low deformability (i.e., high viscosity or low velocity) were separated to side outlets in the microfluidic device, whereas droplets with a small size or high deformability exited to the center outlet. With highspeed imaging, we further identified two sequential droplet deformations during the sorting process and showed that the characteristic distance  $(\delta)$ and the impact angle  $(\theta)$ , which were determined by the physical parameters of droplets, played a regulatory role in deformation-based



droplet sorting. Droplet sorting to the side outlets occurred only when  $\delta \geq 0.542$  or  $\theta \geq 28^{\circ}$ .

## ■ INTRODUCTION

Separation of particles with different physical properties such as size, <sup>1–3</sup> shape, <sup>4,5</sup> or deformability <sup>6</sup> is critical in the food industry, <sup>7</sup> environmental assessment, <sup>8</sup> chemical and biological research, <sup>9</sup> and medical diagnostics. <sup>10</sup> Separation techniques with high selectivity and resolution, for example, are used to separate diseased cells from healthy cells, such as cancer cells<sup>11</sup> or malaria-infected cells. 12,13 A microfluidic-based approach for particle sorting is one of the most effective approaches in the field and has unparalleled advantages due to its fast sorting rate, increased detection accuracy, and reduced sample contamination. 14,15 Microfluidic sorting devices are normally classified as either active or passive sorting devices. Active sorting devices require externally applied force fields such as dielectrophoretic,  $^{16,17}$  optical,  $^{18-20}$  or acoustophoresis  $^{21-23}$  for separation. For some of the approaches, e.g., fluorescence tagging for optical sorting device, particle labeling is also required. Passive sorting devices, on the other hand, do not require extra energy input or additional particle labeling, and the separation process mainly depends on the particle-channel interactions and the intrinsic properties of particles, such as size, shape, shape, density, amass, or deformability, and thus avoids complicated device fabrication needed for active sorting devices.

Deformation-based particle sorting is one of the passive microfluidic sorting approaches and has been studied in mechanical filtration, 26,27 inertial microfluidics, 28,29 and the deterministic lateral displacement (DLD) technique. 1,2 Mechanical filtration technique separates particles by utilizing arrays of pores or funnels in microfluidics, and separation

depends on particle size and deformability. The size of the entrance of the funnel is usually larger than the particle diameter, whereas the size of the exit of funnel is smaller than the particle diameter. Thus, particles with a small diameter or more deformability can escape through the funnel and be separated. The key drawback of the filtration technique is the clogging of nonpermeable particles at the funnel entrance, which, when occurs, significantly reduces the separation efficiency. Inertial microfluidics, on the other hand, use force balance between Dean drag forces and inertial lift forces acting on particles or droplets and are able to separate them based on their size and deformability. However, due to the complexity of the physical basis of the lift forces, many parameters such as the Dean number, channel Reynolds number, particle Reynolds number, and the Stokes number are all needed to be considered when designing the microfluidic channel.<sup>30</sup> Lastly, DLD is a size-dependent sorting technique which uses arrays of obstacles to separate particles to different streamlines. Particles with a diameter larger than the critical diameter will follow the diagonal streamline, whereas small particles follow the center streamline. Because deformation will change the effective size of particles, the DLD method has recently been used to separate particles with different deformability. 31,32 Zhu

Special Issue: Characterization and Applications of Fluidic Devices without Moving Parts

Received: August 30, 2019 Revised: October 18, 2019 Accepted: October 22, 2019 Published: October 22, 2019

<sup>&</sup>lt;sup>†</sup>Department of Materials Science and Engineering, University of California, Davis, Davis, California 95616, United States

<sup>\*</sup>Microsystems Engineering, Rochester Institute of Technology, Rochester, New York 14623, United States

Department of Chemical Engineering, University of California, Davis, Davis, California 95616, United States

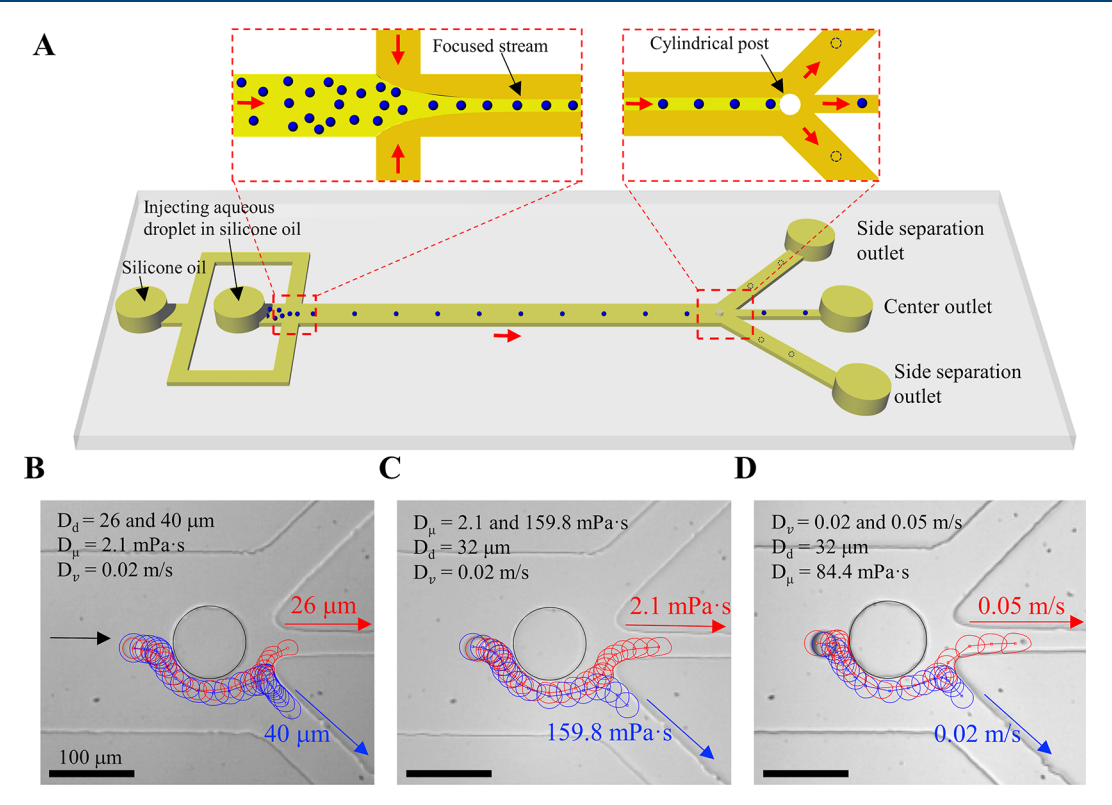


Figure 1. Deformation-based droplet sorting in microfluidics depends on droplet size, viscosity, and velocity. (A). Schematic of the deformation-based droplet sorting in microfluidics. Droplets generated using a microfluidic device (not shown) were collected and injected to the sorting microfluidic device. In the sorting device, droplets were first focused to the centerline of a straight channel, impacted on a cylindrical post, and then exited through either the two side outlets or the center outlet. The gap distance from the post to the center outlet was 40  $\mu$ m. Note that droplet separation refers to the droplets exiting to either of the side outlets. (B), (C), and (D) showed the representative trajectories of droplet sorting by droplet size  $(D_d)$ , droplet viscosity  $(D_u)$ , and droplet velocity  $(D_v)$ , respectively.

et al.,<sup>33</sup> for example, did a numerical study on deformability-based separation with a single obstacle and showed the possibility of cell sorting based on the elastic moduli and the shear modulus of cells. The interplay between particle physical properties, deformation, and sorting, however, remains unclear.

In this work, we designed a microfluidic sorting device with a cylindrical post to provide mechanistic insights of deformation-based droplet sorting and explored the effect of droplet size, viscosity, and velocity on sorting. Careful analysis with high-speed imaging revealed that droplets underwent two sequential deformations: (i) the first deformation upon hitting the post and (ii) the second deformation upon hitting the tip of the outlet. These two deformation processes were related to the characteristic distance  $(\delta)$  and the impact angle  $(\theta)$  that are two decisive parameters in the control of droplet separation. Droplet separation to the side outlets occurred only when  $\delta$  and  $\theta$  were beyond critical values.

### MATERIALS AND METHODS

Microfluidic devices used for droplet generation and sorting were fabricated using the standard soft photolithographic technique. To droplet generation, we implemented a straight flow-focusing channel ( $W = 260 \, \mu \text{m}$ ,  $H = 40 \, \mu \text{m}$ ) connected to two inlets and one outlet, as described in our previous study. For droplet sorting, a microfluidic device with a cylindrical post was used (Figure 1). The sorting device was composed of a flow-focusing geometry with two inlets, a straight-focusing channel ( $W = 260 \, \mu \text{m}$ ,  $H = 40 \, \mu \text{m}$ ), and a cylindrical post (diameter =  $100 \, \mu \text{m}$ ) near the three outlets (one centerchannel with the width of  $40 \, \mu \text{m}$  and two side-channels with

the width of 100  $\mu$ m). The gap distance from the post to the entrance of the center outlet was 40  $\mu$ m. For both droplet generation and sorting devices, the inlets of the device were connected to the plastic syringes (1 and 10 mL, BD Luer-Lok) filled with either continuous or dispersed phases with polyethylene tubing (BB31695-PE/2, Scientific Commodities Inc., AZ, USA). These syringes were mounted on two syringe pumps (Harvard Apparatus, Pump 11 Elite, MA, USA). The same tubing was used to connect the outlets of the device to the glass vials to collect the generated or sorted droplets.

The continuous phase for both droplet generation and sorting was composed of 98 wt % 50 cSt silicone oil and 2 wt % RSN-749 fluid (Dow Corning, MI, USA). The dispersed phase contained deionized (DI) water, 0.5 wt % sodium dodecyl sulfate (SDS), and glycerol with varied concentrations (25, 45, 62, 80, 85, and 90 wt %, which corresponded to droplet viscosity of 2.1, 5.7, 9.7, 49.3, 84.4, and 159.8 mPa·s, respectively). Density and surface tension<sup>36</sup> of droplets were measured, and the values are listed in Table S1. Viscosity of droplets was measured using a rheometer (Discovery HR-2, TA Instruments, DE, USA). To generate droplets with the size ranging from 26 to 40  $\mu$ m, a flow rate ratio of continuous and dispersed phases was set from 105:1 to 80:1. The generated droplets were then collected in a reservoir and injected into the microfluidic sorting device. The ratio of flow rates of the continuous phase and droplets in the sorting device was set at 0.4:12, 0.6:18, 1.0:24, and 1.5:30, corresponding to the velocity of 0.02, 0.03, 0.04, and 0.05 m/s, respectively. When setting a new flow rate, the system was run for at least 200 s to reach equilibrium. Prior to experiments, the continuous phase was

**Industrial & Engineering Chemistry Research** 

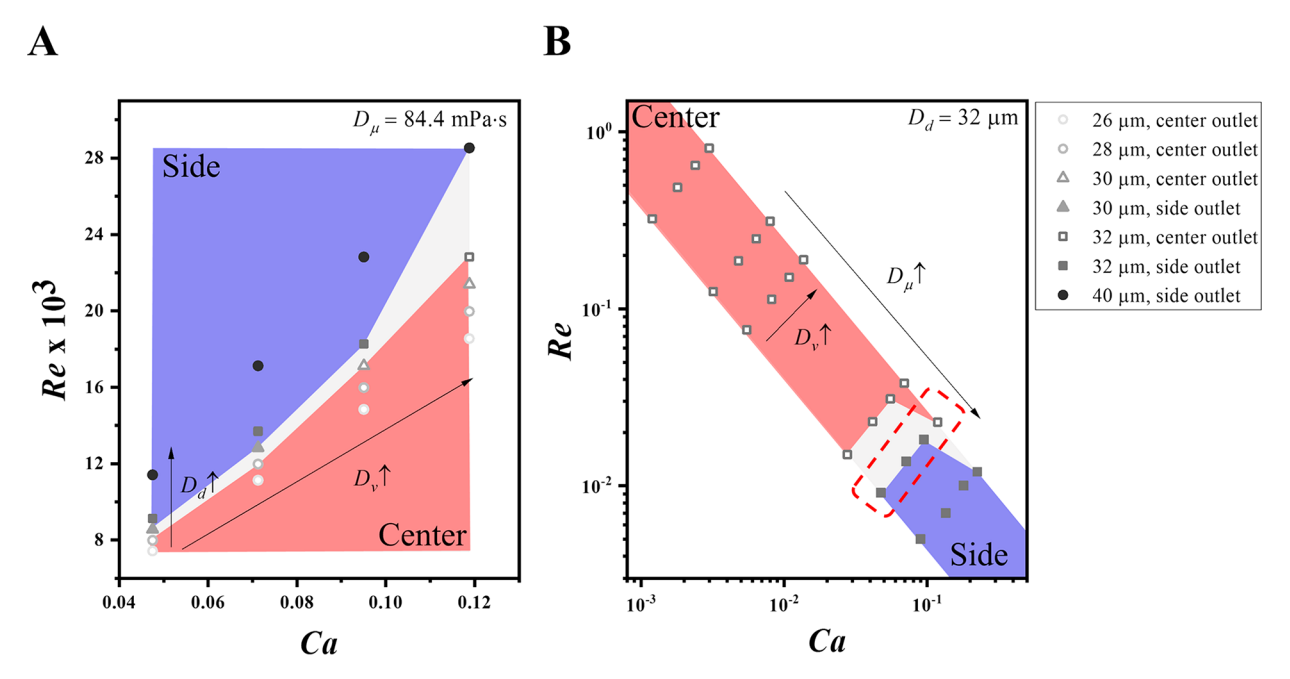


Figure 2. Transition regions for droplet sorting. (A).  $D_d$  and  $D_v$  dependent droplet separation at a constant viscosity ( $D_\mu = 84.4 \text{ mPa·s}$ ).  $D_d$  regulated droplet separation such that small droplets ( $D_d = 26 \text{ and } 28 \mu\text{m}$ ) exited to the center outlet and large droplets ( $D_d = 40 \mu\text{m}$ ) were separated to the side outlets.  $D_v$  dependent droplet separation was observed when  $D_d = 30 \text{ and } 32 \mu\text{m}$ . Droplets with low  $D_v$  were separated to the side outlets, whereas droplets with high  $D_v$  exited through the center outlet. Note that a gray band between center (red) and side (blue) represents the transition regime. (B).  $D_\mu$  and  $D_v$  dependent droplet separation at a constant size ( $D_d = 32 \mu\text{m}$ ). As  $D_\mu$  increased, droplets were separated to the side outlets. Only when  $D_\mu = 84.4 \text{ mPa·s}$  (dashed box),  $D_v$  dependent droplet separation was observed, such that as we increased  $D_v$  droplets exited through the center outlet.

filtered by a microscale filter. All chemicals except RSN-749 fluid were purchased from Sigma-Aldrich (MO, USA).

A high-speed digital camera (Phantom VEO-710L, Vision Research, NJ, USA) equipped with an optical microscope (AmScope, CA, USA) was used to monitor the generation and sorting of droplets and the dynamic deformation of droplets upon hitting the post and the tip of the outlet. The camera was interfaced to Phantom PCC software, which was employed to capture the images at a speed of 3000 frames per second. Fluid streamlines inside microfluidic channel were simulated using COMSOL Multiphysics software.

### ■ RESULTS AND DISCUSSION

We injected droplets with specific droplet size  $(D_d)$  and viscosity  $(D_u)$  to the microfluidic sorting device in the presence of a flow-focusing stream, which enabled the droplets to follow the center streamline and impact the center of the post (Figure 1A). We also varied droplet velocity  $(D_{\nu})$  by changing the flow rates of the continuous and dispersed phases as described in the Materials and Methods section. Depending on  $D_d$ ,  $D_w$  and  $D_v$ , we found that droplets either exited through the center outlet or were sorted to the side outlets after hitting the post (Figure 1B,C,D). Fluid streamlines with and without the post were simulated (Figure S1A,B), which show how the fluid streamline is affected by the post. Here we defined "droplet separation" as droplets being sorted to the side outlets. Note that the two side outlets were symmetric; therefore, the chance of droplets being sorted to either side outlet was the same.

To understand how these physical parameters of droplets played a role in the sorting process, we plotted the results using two dimensionless numbers (Figure 2A,B): the Reynolds number ( $Re \equiv \rho D_{\nu} D_{d}/D_{u}$ ) and the capillary number ( $Ca \equiv \frac{1}{2} \frac{1}{2}$ 

 $D_{\nu}D_{\nu}/\sigma$ ), where  $\rho$  was the density of a droplet and  $\sigma$  was the surface tension of a droplet. Note that Re and Ca used here were calculated based on the size, viscosity, and velocity of the droplet rather than the properties of fluids in the continuous phase. Calculated values for Re and Ca were listed in Table S1. We first examined the effect of  $D_d$  and  $D_v$  on droplet sorting and analyzed sorting results using droplets with  $D_{\mu} = 84.4$ mPa·s but with varied  $D_d$  and  $D_v$  (Figure 2A). The results showed that in the tested range of Re (0.007-0.029) and Ca (0.048-0.119),  $D_d$  regulated droplet separation. All droplets with  $D_d$  = 26 and 28  $\mu$ m exited through the center outlet, and droplets with  $D_d$  = 40  $\mu m$  were separated to the side outlets. For droplets with  $D_d$  = 30 and 32  $\mu$ m, however,  $D_{\nu}$  regulated droplet separation. Taking  $D_d = 32 \mu m$  as an example, droplets were separated to the side outlets when  $D_{\nu}$  was less than or equal to 0.04 m/s (i.e., Ca = 0.095) but exited to the center outlet when  $D_v$  was 0.05 m/s (i.e., Ca = 0.119). A similar trend was also observed for droplets with  $D_d$  = 30  $\mu$ m. These results suggested that the changes in both  $D_d$  and  $D_v$  influenced droplet separation. According to the DLD method, particles with different radii will follow different streamlines in a laminar flow through a periodic array of obstacles. For instance, small particles followed the center streamline, whereas large particles showed lateral displacement from the center streamline, resulting in separation. At high  $D_{\nu}$ , we hypothesize that droplet deformation induced a decrease in effective  $D_d$ , which allowed droplets to follow the center streamline and exit through the center outlet. To confirm the hypothesis, we analyzed the sorting results using droplets with  $D_d = 32 \mu m$  but with varying  $D_u$  and  $D_v$  (Figure 2B). The results showed that as we increased  $D_u$  to above 84.4 mPa·s, droplets started to separate to the side outlets. However, as we increased  $D_{\nu}$  (i.e., increased Ca), while keeping  $D_{\mu}$  constant at 84.4 mPa·s

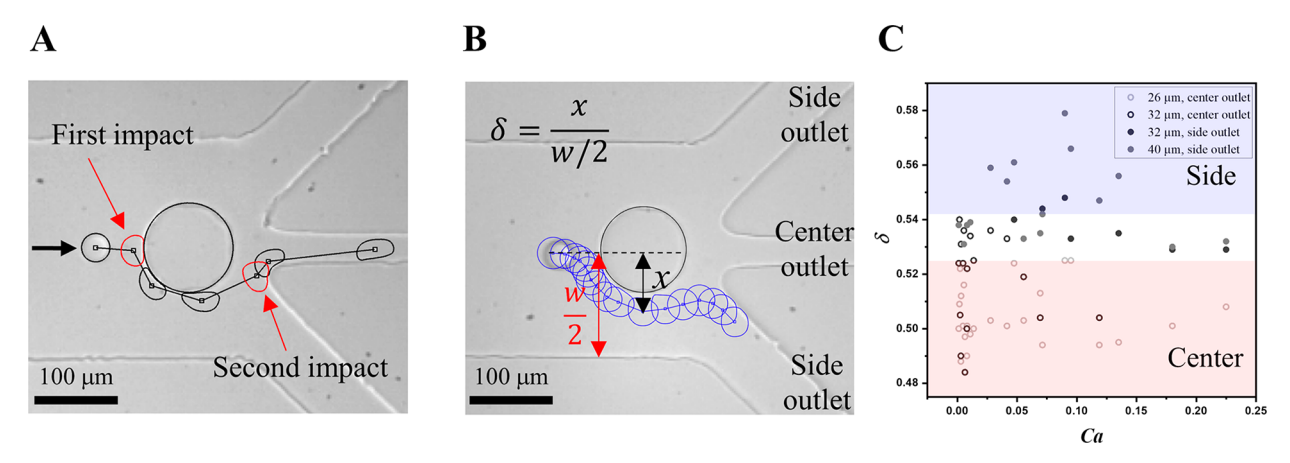


Figure 3. Characteristic distance,  $\delta$ , contributes to droplet sorting. (A). Trajectory of a droplet showing two sequential deformations before entering the center outlet. (B). Representative image showing the trajectory of droplet and  $\delta$  which was defined as the ratio of the distance between the center of the post and the center of mass of the droplet, x, to the channel wall, w/2. (C). There was a minimum  $\delta$  ( $\delta$  = 0.542) beyond which droplets were separated to the side outlets and a maximum  $\delta$  ( $\delta$  = 0.525) below which droplets exited through the center outlet. Droplet separation was not predictable in the regime where  $\delta$  = 0.525–0.542.

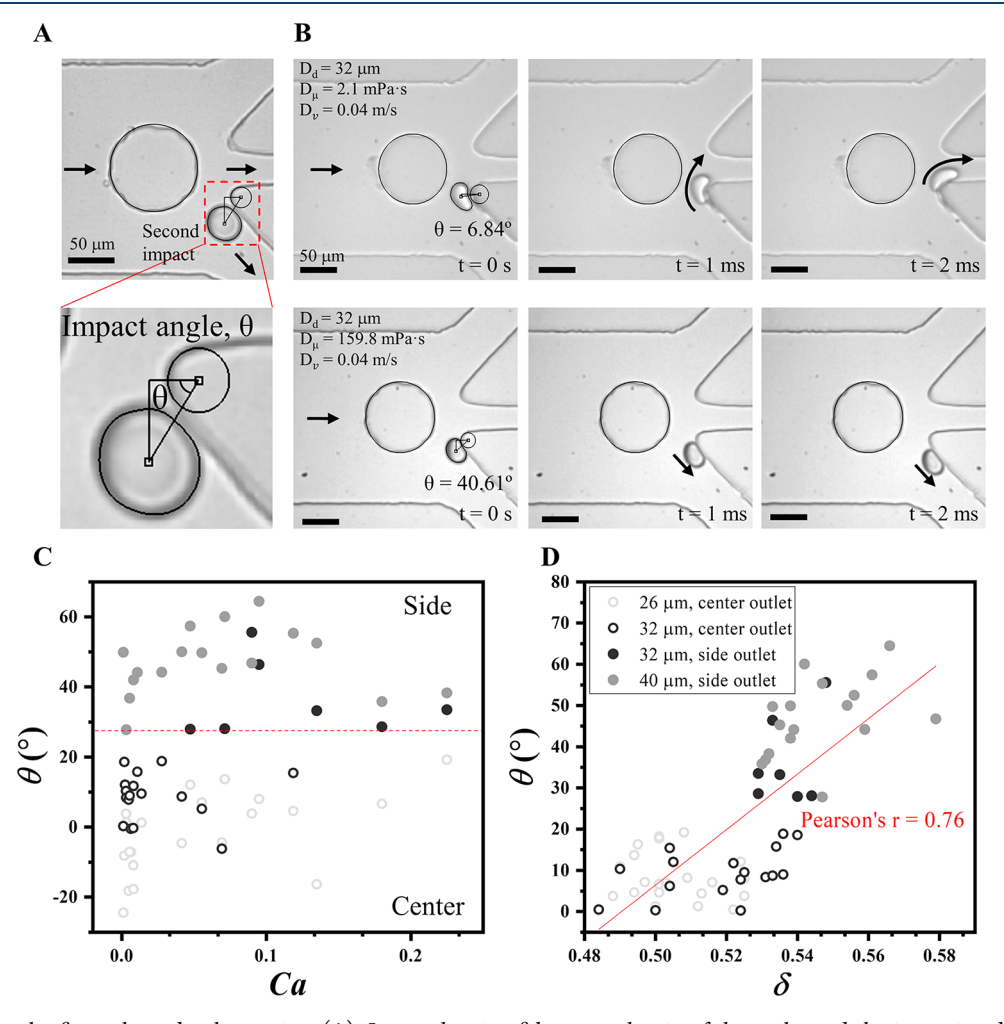


Figure 4. Impact angle,  $\theta$ , regulates droplet sorting. (A). Image showing  $\theta$  between the tip of the outlet and the impacting droplet. (B). Time-dependent image of droplet separation after impacting on the central sorting channel. (Top) The droplet with a small  $\theta$  climbed up to the center separation outlet, and (bottom) the droplet with a large  $\theta$  slid down to the side outlets. (C). Droplets were sorted to the side outlets when  $\theta$  was larger than the critical impact angle,  $\theta_c = 28^\circ$ . (D). Linear correlation between  $\delta$  and  $\theta$ . The correlation coefficient was 0.76.

(dashed box in Figure 2B), droplets started to exit through the center outlet. Because decreasing  $D_{\mu}$  or increasing  $D_{\nu}$  results in decreasing the effective  $D_{d}$  <sup>37</sup> the reduced effective  $D_{d}$  caused

droplets to exit through the center outlet. The change in the effective  $D_d$  thus has an analogous effect as changing  $D_d$  on droplet separation.

We further verified effective  $D_d$  by examining droplet deformation using high-speed imaging. We showed that droplets experienced two sequential deformations: (i) deformation upon the first impact at the post and (ii) deformation upon the second impact at the tip of the outlet (Figure 3A). We observed that while droplets moved along the post after the first impact, the distance from the center of the post to the center of mass of the droplet influenced droplet separation. We defined such a distance as the characteristic distance,  $\delta$ , where  $\delta = x/(w/2)$  (Figure 3B). x is the distance between the center of the post and the center of mass of the droplet, and w is the channel width. We showed that, when the gap distance between the post and the outlet was 40  $\mu$ m, there was a minimum  $\delta$  ( $\delta$  = 0.542) beyond which the droplets were separated to the side outlets. Droplets exited through the center outlet when  $\delta$  was below a maximum  $\delta$  ( $\delta$  = 0.525) (Figure 3C). Note that there was a regime of  $\delta$  (0.525–0.542) during which droplet separation was not predictable. Because x is related to the effective  $D_d$  upon hitting the post, any changes of  $D_d$ ,  $D_w$  and  $D_v$  that decreased the effective  $D_d$  will decrease x, resulting in a decreased  $\delta$  and leading to the exiting of droplets to the center outlet. The results agreed with the numerical study by Kruger et al.<sup>31</sup> where more deformable cells had a smaller  $D_{\perp}$  (analogous to  $\delta$ ) and followed the center streamline. Whereas less deformable cells with a bigger  $D_{\perp}$ showed a larger deviation from the center streamline. It is worth noting that the absolute values of droplet and post diameter need to be considered in designing the sorting device. When the post diameter decreases while  $\delta$  keeps constant, for example, critical x, i.e., x below which all streamline will exit through the center outlet, decreases, resulting in droplet sorting to the side outlet (Figure S2A,B).

To investigate droplet deformation upon the second impact at the tip of the outlet, we analyzed the impact angle,  $\theta$ , between the tip of the outlet and the center of mass of the impacting droplet, as shown in Figure 4A.  $\theta$  was measured when droplets hit the tip of the outlet and deformed against the channel wall. We noticed that during the impact at the tip of the outlet, the center of mass of a droplet could shift upward or downward leading to droplet separation. The timedependent droplet deformation and sorting images were shown in Figure 4B. When  $D_u$  was small, e.g.,  $D_u = 2.1$  mPa· s, the droplet impacted the tip of the outlet with  $\theta = 6.84^{\circ}$ , and subsequently the center of mass of the droplet moved upward. As a result, the droplet climbed up the tip and exited through the center outlet. When  $D_u$  was increased to 159.8 mPa·s, the center of mass of the droplet moved downward with  $\theta$  = 40.61°, and the droplet slid down to the side outlets. We plotted  $\theta$  as Ca for droplets with varied  $D_d$ ,  $D_{\mu\nu}$  and  $D_{\nu}$  and found that there was a critical impact angle,  $\theta_c = 28^{\circ}$ , beyond which droplets with  $D_d$  = 32 and 40  $\mu$ m were separated to the side outlets (Figure 4C). Note that  $D_d = 26 \,\mu\text{m}$  droplets always impacted the tip of the outlet with  $\theta$  lower than  $\theta_c$  and exited through the center outlet. In addition, as  $\delta$  was determined by the physical properties of droplets,  $\theta$  was also regulated by droplet properties. Thus,  $\theta$  was linearly related to  $\delta$  with a correlation coefficient of 0.76, as shown in Figure 4D. When  $\delta$ was small,  $\theta$  also tended to be small and vice versa. This correlation agreed with the numerical study done by Zhu et al.<sup>33</sup> where they showed that as the deformability of capsule increased, the distance between the obstacle and the center of mass of the capsule decreased (analogous to decrease in  $\delta$ ).

Thus, the trajectory of such a capsule after hitting the obstacle deviated less from the center streamline, which led to a small  $\theta$ .

Last, it is worth noting that the gap distance also played a role in droplet separation. When the gap distance was increased to 50  $\mu$ m, for example, all droplets with 26 and 32  $\mu$ m did not have the second impact at the tip of the outlet and exited through the center outlet as shown in Figure S3A. When  $D_d=40~\mu$ m, droplets showed the second impact and were separated to the side outlets depending on  $D_\mu$  and  $D_\nu$ . The critical  $\theta$  was 27° in this case (Figure S3B). As we further increased the gap distance to 85, 90, or 95  $\mu$ m (Figure S3C), all droplets with  $D_d=26$ , 32, and 40  $\mu$ m were guided to the center outlet, and no observable droplet separation occurred. These results could be explained by the characteristic laminar flow in microfluidics<sup>38</sup> and indicated that the gap distance between the post and the outlet should be optimized for future sorting devices.

### CONCLUSION

We showed a microfluidic sorting device with a cylindrical post that could separate droplets depending on droplet properties, such as  $D_d$ ,  $D_w$ , and  $D_v$ , and identified two physical parameters during droplet deformation, e.g., characteristic distance,  $\delta$ , and impact angle,  $\theta$ , that were determined by droplet properties and regulated deformation-based droplet sorting. We showed that as  $D_{\mu}$  was increased or  $D_{\nu}$  was decreased, droplets had a large effective  $D_d$  during deformation, leading to a large  $\delta$  and  $\theta$ . As a result, droplets followed the same trajectories of large droplets and were separated to the side outlets. The present study provided a mechanistic understanding of the relation between droplet properties and deformation-based sorting and thus offered useful guidelines for future design of microfluidicbased sorting devices. We speculate that such devices will also be applicable for separation of trains of drops, given that the distance between droplets is controlled. In addition, we expect that additional posts along the flow direction will amplify the displacement of droplets with different impact angles as we observed here and thus may improve the sorting process. Further studies using droplets with viscoelastic properties would convey critical information for a thorough understanding on the influence of  $\delta$  and  $\theta$  on the droplet separation, which, in turn, will enable us to design a simple yet effective sorting device for cell sorting and medical diagnosis.

### ASSOCIATED CONTENT

## **S** Supporting Information

The Supporting Information is available free of charge on the ACS Publications website at DOI: 10.1021/acs.iecr.9b04823.

Re and Ca calculation table, simulation of fluid streamline, droplet separation with 50, 85, 90, and 95  $\mu$ m gap distance sorting device (PDF)

### AUTHOR INFORMATION

#### Corresponding Author

\*E-mail: jdwan@ucdavis.edu. Phone: 530-754-0895.

ORCID ®

Yunju Chang: 0000-0003-2588-3762

### **Author Contributions**

All authors have given approval to the final version of the manuscript.

### **Funding**

J.W. received funding from NSF grant CBET-1649993.

#### Notes

The authors declare no competing financial interest.

#### ACKNOWLEDGMENTS

The authors thank NSF (CBET-1649993) for the financial support of this work. We thank Dr. Saif Islam for helping with simulating fluid streamline inside the sorting device.

### REFERENCES

- (1) Huang, L. R.; Cox, E. C.; Austin, R. H.; Sturm, J. C. Continuous Particle Separation Through Deterministic Lateral Displacement. *Science* **2004**, 304, 987–990.
- (2) Inglis, D. W.; Davis, J. A.; Austin, R. H.; Sturm, J. C. Critical Particle Size for Fractionation by Deterministic Lateral Displacement. *Lab Chip* **2006**, *6*, 655–658.
- (3) Yamada, M.; Nakashima, M.; Seki, M. Pinched Flow Fractionation: Continuous Size Separation of Particles Utilizing a Laminar Flow Profile in a Pinched Microchannel. *Anal. Chem.* **2004**, 76, 5465–5471.
- (4) Li, M.; Muñoz, H. E.; Goda, K.; Di Carlo, D. Shape-Based Separation of Microalga Euglena Gracilis Using Inertial Microfluidics. *Sci. Rep.* **2017**, *7*, 10802.
- (5) Masaeli, M.; Sollier, E.; Amini, H.; Mao, W.; Camacho, K.; Doshi, N.; Mitragotri, S.; Alexeev, A.; Di Carlo, D. Continuous Inertial Focusing and Separation of Particles by Shape. *Phys. Rev. X* **2012**, *2*, 031017.
- (6) Preira, P.; Grandné, V.; Forel, J. M.; Gabriele, S.; Camara, M.; Theodoly, O. Passive Circulating Cell Sorting by Deformability Using a Microfluidic Gradual Filter. *Lab Chip* **2013**, *13*, 161–170.
- (7) Pyle, B. H.; Broadaway, S. C.; McFeters, G. A. Sensitive Detection of Escherichia Coli O157:H7 in Food and Water by Immunomagnetic Separation and Solid-Phase Laser Cytometry. *Appl. Environ. Microbiol.* **1999**, *65*, 1966–1972.
- (8) Klaine, S. J.; Alvarez, P. J. J.; Batley, G. E.; Fernandes, T. F.; Handy, R. D.; Lyon, D. Y.; Mahendra, S.; McLaughlin, M. J.; Lead, J. R. Nanomaterials in the Environment: Behavior, Fate, Bioavailability, and Effects. *Environ. Toxicol. Chem.* **2008**, 27, 1825–1851.
- (9) Gossett, D. R.; Weaver, W. M.; MacH, A. J.; Hur, S. C.; Tse, H. T. K.; Lee, W.; Amini, H.; Di Carlo, D. Label-Free Cell Separation and Sorting in Microfluidic Systems. *Anal. Bioanal. Chem.* **2010**, 397, 3249–3267.
- (10) Olsvik, Ø.; Popovic, T.; Skjerve, E.; Cudjoe, K. S.; Hornes, E.; Ugelstad, J.; Uhlén, M. Magnetic Separation Techniques in Diagnostic Microbiology. *Clin. Microbiol. Rev.* **1994**, *7*, 43–54.
- (11) Nagrath, S.; Sequist, L. V.; Maheswaran, S.; Bell, D. W.; Irimia, D.; Ulkus, L.; Smith, M. R.; Kwak, E. L.; Digumarthy, S.; Muzikansky, A.; et al. Isolation of Rare Circulating Tumour Cells in Cancer Patients by Microchip Technology. *Nature* **2007**, *450*, 1235–1239.
- (12) Gascoyne, P.; Mahidol, C.; Ruchirawat, M.; Satayavivad, J.; Watcharasit, P.; Becker, F. F. Microsample Preparation by Dielectrophoresis: Isolation of Malaria. *Lab Chip* **2002**, *2*, 70–75.
- (13) Gascoyne, P.; Satayavivad, J.; Ruchirawat, M. Microfluidic Approaches to Malaria Detection. *Acta Trop.* **2004**, *89*, 357–369.
- (14) Chin, C. D.; Linder, V.; Sia, S. K. Lab-on-a-Chip Devices for Global Health: Past Studies and Future Opportunities. *Lab Chip* **2007**, *7*, 41–57.
- (15) Nam, J. M.; Thaxton, C. S.; Mirkin, C. A. Nanoparticle-Based Bio-Bar Codes for the Ultrasensitive Detection of Proteins. *Science* **2003**, *301*, 1884–1886.
- (16) Dürr, M.; Kentsch, J.; Müller, T.; Schnelle, T.; Stelzle, M. Microdevices for Manipulation and Accumulation of Micro- and Nanoparticles by Dielectrophoresis. *Electrophoresis* **2003**, *24*, 722–731.
- (17) Pethig, R. Dielectrophoresis: Using Inhomogeneous AC Electrical Fields to Separate and Manipulate Cells. *Crit. Rev. Biotechnol.* **1996**, *16*, 331–348.

- (18) MacDonald, M. P.; Spalding, G. C.; Dholakia, K. Microfluidic Sorting in an Optical Lattice. *Nature* **2003**, *426*, 421–424.
- (19) Wang, M. M.; Tu, E.; Raymond, D. E.; Yang, J. M.; Zhang, H.; Hagen, N.; Dees, B.; Mercer, E. M.; Forster, A. H.; Kariv, I.; et al. Microfluidic Sorting of Mammalian Cells by Optical Force Switching. *Nat. Biotechnol.* **2005**, *23*, 83–87.
- (20) Baret, J. C.; Miller, O. J.; Taly, V.; Ryckelynck, M.; El-Harrak, A.; Frenz, L.; Rick, C.; Samuels, M. L.; Hutchison, J. B.; Agresti, J. J.; et al. Fluorescence-Activated Droplet Sorting (FADS): Efficient Microfluidic Cell Sorting Based on Enzymatic Activity. *Lab Chip* **2009**, *9*, 1850–1858.
- (21) Laurell, T.; Petersson, F.; Nilsson, A. Chip Integrated Strategies for Acoustic Separation and Manipulation of Cells and Particles. *Chem. Soc. Rev.* **2007**, *36*, 492–506.
- (22) Augustsson, P.; Magnusson, C.; Nordin, M.; Lilja, H.; Laurell, T. Microfluidic, Label-Free Enrichment of Prostate Cancer Cells in Blood Based on Acoustophoresis. *Anal. Chem.* **2012**, *84*, 7954–7962.
- (23) Antfolk, M.; Antfolk, C.; Lilja, H.; Laurell, T.; Augustsson, P. A Single Inlet Two-Stage Acoustophoresis Chip Enabling Tumor Cell Enrichment from White Blood Cells. *Lab Chip* **2015**, *15*, 2102–2109.
- (24) Hsu, C. H.; Di Carlo, D.; Chen, C.; Irimia, D.; Toner, M. Microvortex for Focusing, Guiding and Sorting of Particles. *Lab Chip* **2008**, *8*, 2128–2134.
- (25) Huh, D.; Bahng, J. H.; Ling, Y.; Wei, H. H.; Kripfgans, O. D.; Fowlkes, J. B.; Grotberg, J. B.; Takayama, S. Gravity-Driven Microfluidic Particle Sorting Device with Hydrodynamic Separation Amplification. *Anal. Chem.* **2007**, *79*, 1369–1376.
- (26) McFaul, S. M.; Lin, B. K.; Ma, H. Cell Separation Based on Size and Deformability Using Microfluidic Funnel Ratchets. *Lab Chip* **2012**, *12*, 2369–2376.
- (27) Preira, P.; Grandné, V.; Forel, J. M.; Gabriele, S.; Camara, M.; Theodoly, O. Passive Circulating Cell Sorting by Deformability Using a Microfluidic Gradual Filter. *Lab Chip* **2013**, *13*, 161–170.
- (28) Di Carlo, D.; Irimia, D.; Tompkins, R. G.; Toner, M. Continuous Inertial Focusing, Ordering, and Separation of Particles in Microchannels. *Proc. Natl. Acad. Sci. U. S. A.* **2007**, *104*, 18892–18897
- (29) Hur, S. C.; Henderson-Maclennan, N. K.; McCabe, E. R. B.; Di Carlo, D. Deformability-Based Cell Classification and Enrichment Using Inertial Microfluidics. *Lab Chip* **2011**, *11*, 912–920.
- (30) Wu, Z.; Willing, B.; Bjerketorp, J.; Jansson, J. K.; Hjort, K. Soft Inertial Microfluidics for High Throughput Separation of Bacteria from Human Blood Cells. *Lab Chip* **2009**, *9*, 1193–1199.
- (31) Krüger, T.; Holmes, D.; Coveney, P. V. Deformability-Based Red Blood Cell Separation in Deterministic Lateral Displacement Devices-A Simulation Study. *Biomicrofluidics* **2014**, *8*, 054114.
- (32) Ye, S.; Shao, X.; Yu, Z.; Yu, W. Effects of the Particle Deformability on the Critical Separation Diameter in the Deterministic Lateral Displacement Device. *J. Fluid Mech.* **2014**, 743, 60–74.
- (33) Zhu, L.; Rorai, C.; Dhrubaditya, M.; Brandt, L. A Microfluidic Device to Sort Capsules by Deformability: A Numerical Study. *Soft Matter* **2014**, *10*, 7705–7711.
- (34) Xia, Y.; Whitesides, G. M. Soft Lithography. Annu. Rev. Mater. Sci. 1998, 28, 153-184.
- (35) Wan, J.; Shi, L.; Benson, B.; Bruzek, M. J.; Anthony, J. E.; Sinko, P. J.; Prudhomme, R. K.; Stone, H. A. Microfluidic Generation of Droplets with a High Loading of Nanoparticles. *Langmuir* **2012**, 28, 13143–13148.
- (36) Gianino, C. Measurement of surface tension by the dripping from a needle. *Phys. Educ.* **2006**, *41*, 440–444.
- (37) Beech, J. P.; Holm, S. H.; Adolfsson, K.; Tegenfeldt, J. O. Sorting Cells by Size, Shape and Deformability. *Lab Chip* **2012**, *12*, 1048–1051.
- (38) Sharp, K. V.; Yazdi, S. H.; Davison, S. M. Localized Flow Control in Microchannels Using Induced-Charge Electroosmosis near Conductive Obstacles. *Microfluid. Nanofluid.* **2011**, *10*, 1257–1267.